



**HAL**  
open science

## Dislocation emission at the onset of plasticity during nanoindentation in gold

Esther Carrasco, Oscar Rodríguez de La Fuente, Juan M. Rojo

► **To cite this version:**

Esther Carrasco, Oscar Rodríguez de La Fuente, Juan M. Rojo. Dislocation emission at the onset of plasticity during nanoindentation in gold. *Philosophical Magazine*, 2008, 88 (03), pp.281-296. 10.1080/14786430701798951 . hal-00513848

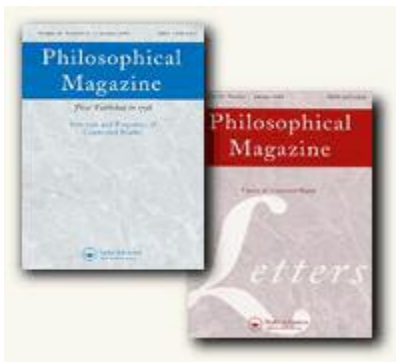
**HAL Id: hal-00513848**

**<https://hal.science/hal-00513848>**

Submitted on 1 Sep 2010

**HAL** is a multi-disciplinary open access archive for the deposit and dissemination of scientific research documents, whether they are published or not. The documents may come from teaching and research institutions in France or abroad, or from public or private research centers.

L'archive ouverte pluridisciplinaire **HAL**, est destinée au dépôt et à la diffusion de documents scientifiques de niveau recherche, publiés ou non, émanant des établissements d'enseignement et de recherche français ou étrangers, des laboratoires publics ou privés.



**Dislocation emission at the onset of plasticity during nanoindentation in gold**

Journal:	<i>Philosophical Magazine &amp; Philosophical Magazine Letters</i>
Manuscript ID:	TPHM-07-Jun-0188.R1
Journal Selection:	Philosophical Magazine
Date Submitted by the Author:	06-Nov-2007
Complete List of Authors:	Carrasco, Esther; Universidad Complutense, Física de Materiales Rodríguez de la Fuente, Oscar; Universidad Complutense, Física de Materiales Rojo, Juan M.; Universidad Complutense, Física de Materiales
Keywords:	dislocations, plasticity of crystals
Keywords (user supplied):	scanning tunnelling microscopy, surface defects, gold



Catchline (head of first page only) *Philosophical Magazine*, Vol. X, No. X, Month 2007, xxx–xxx

Running heads (verso) *E. Carrasco et al.*  
(recto) *Dislocation emission at the onset of plasticity*

## Article Type

# Dislocation emission at the onset of plasticity during nanoindentation in gold

E. CARRASCO\*, O. RODRÍGUEZ DE LA FUENTE and J. M. ROJO

Departamento de Física de Materiales. Universidad Complutense, 28040 Madrid, Spain

\*Corresponding author. Email: esthercarrasco@fis.ucm.es

Nanoindentations and the subsequent plastic damage in the form of dislocation configurations have been both generated and imaged with Scanning Tunnelling Microscopy (STM) on a reconstructed Au(001) surface, the resulting observations being interpreted in terms of ~~an analysis based on~~ the elastic theory of dislocations in a continuum. The ~~rearranged~~ pileup material around the nanoindentation is described in terms of dislocation emission and glide involving, in particular, multiple cross-slip. 'Mesas', shallow protusions stemming from a special dislocation configuration consisting of Schockley partial dislocations encompassing two stacking faults, are shown to glide parallel to the surface under the stress generated by further nanoindentations. ~~The motion (glide) of 'mesas' under the stress generated by further nanoindentations is demonstrated.~~ The spatial distribution of 'mesas' around the nanoindentation traces is shown to be controlled by ~~by a balance between~~ the interactions between the different 'mesas' and the stresses arising from the nanoindentation itself.

*Keywords:* Dislocations, crystal plasticity, scanning tunneling microscopy, gold, surface defects

*AMS Subject Classification:*

## 1. Introduction

Nanoindentation, in conjunction with surface sensitive techniques, such as atomic force microscopies (AFM), is currently being used to study the elastic-plastic transition at the nanoscale and examine the dislocations and related defects involved in ~~the these~~ first stages of plasticity [1-6]. Apart of its intrinsic interest for the elucidation of the role of surfaces in the mechanical properties of solids, these studies are particularly relevant in view of the growing interest in the physical properties of nanostructures. Furthermore, a detailed knowledge of the plastic deformation mechanisms is highly desirable in relation to friction processes in the wear regime. Nanoindentation experiments are often complemented by atomistic simulations [5], [7-11]. Although a number of mechanisms related to the incipient stages of plasticity have been elucidated, the atomic processes taking place at the initial stages of plasticity in solid surfaces still contain many uncertainties

[4]. In particular, more information would be required about the parameters and geometry of the dislocations created during the plastic stage and about the mechanisms involved in their nucleation.

In recent times, we have shown [12] that, in some cases, the same STM tip can be used to carry out, first, nanoscale indents ~~the nanoindentation~~ and, then, the image. This allows an a close ~~in-situ~~ correlation between nanoindentation stresses and defects produced thereby. Other techniques allow both the force measurement together with surface imaging capabilities. This is the case for nanoindentation with AFM or, for example, with Hysitron systems [1]. However, ~~But~~ STM has a (generally) higher spatial resolution, which has allowed us to identify small defect configurations. Using this approach, we have shown that two special types of dislocation configurations are generated around ~~naoindentation-latter~~: ‘mesas’ and ‘screw-loops’<sup>†</sup>, both of which intersect the surface and give rise to permanent features that can be disclosed by STM [13-14]. By complementing those studies with AFM, we have also correlated the generation of those defects with the displacement bursts (sometimes called ‘pop-ins’) in the AFM-generated force vs penetration curves [15]. Here, we present new results about the kinematics and dynamics of both ‘mesas’ and ‘screw-loops’ obtained by STM observations supported by an analysis based on the elastic theory of dislocations in a continuum. In particular, we report and account for the spatial distribution of ‘mesas’ around the nanoindentation traces, we analyse the motion of ‘mesas’ under the stresses generated by further nanoindentations or by pre-existing neighbour dislocations and we explain how terraces and permanent traces (craters and pile-up) around the nanoindentation are generated by a dislocation mechanism involving dislocation generation and subsequent multiple cross-slip. Our results imply that the theory of dislocations in a continuum can be used with confidence to describe a number of processes involving dislocations at the crystal surface. They may also open the way to a better understanding of the role of the surface in the generation of dislocations in a solid. Two types of incipient plastic events occurring in a surface are also disclosed: a mechanism of dislocation-mediated mass transport along the surface from the indentation point (‘mesas’ glide) and another one involving the generation of pileup material due to glide and cross-slip of ‘screw-loops’.

## 2. Experimental procedure

A conventional ultrahigh-vacuum chamber equipped with Auger electron spectroscopy (AES), low energy electron diffraction (LEED) and a homemade scanning tunnelling microscope (STM) was used. Au(001) surfaces were prepared by the standard combination of Ar<sup>+</sup> ion bombardment plus ~~and~~ high temperature annealing ~~and were analysed at room temperature~~. All the STM images shown in this paper were obtained ~~with the sample at 300K~~ in the constant-current mode with values of tunnel currents of the order of 0.1 nA and negative bias voltages in the 0.1 V range applied to the sample. STM tips were prepared from tungsten wires by electrolysis following conventional wisdom. Images of the tips were obtained by scanning electron microscopy (SEM); they showed that tips ends were spherical in shape with a radius about 70 nm.

Nanoscale indents (in the following designed as nanoindentations) ~~Nanoindentations~~ were performed with the STM by letting tips progress towards the sample once the tunnelling current had been established. The same tips are used to probe the reconstructed Au(001) sample. The initial tunnelling current (~0.1 nA) and bias voltage are selected at fixed values in the electronics controls. Then the nanoindentation procedure is done manually with the feedback switched off, by approaching the tip to the surface and retracting it as soon

<sup>†</sup> ‘Mesas’ are shallow protrusions stemming from a special dislocation configuration consisting of two pairs of Shockley partial dislocations encompassing two stacking faults on adjacent planes (See scheme in Fig.1). ‘Screw-loops’ refer to half-loops (i.e. intersecting the surface) with a screw component for the segments emerging at the surface. It is clear that only some segments of the loops can be in the screw orientation. See reference 16.

as the tunnelling current reaches a saturation value. Once the nanoindentation is performed, the feedback is connected again and an image is acquired. ~~this procedure, we estimate the deformation rate to be a few nanometers per second. The reproducibility of the nanoindentation with STM has been already shown [16].~~ During the process both the tunnel current and bias voltage are maintained fixed. By selecting different bias voltages, the size of the permanent traces (craters) left over by the nanoindentation can be controlled for a wide variety of tips ~~in such a way that~~. By decreasing voltages in the range 2 V - 0.01 V the size of the nanoindentation traces, as characterised by their linear dimensions, can be increased in the range of approximately 20 nm to 150 nm. ~~Although with this technique, neither the incremental nor the total load can be measured, the reproducibility of the nanoindentation traces as analysed by STM has already been shown [16].~~

### 3. Results and discussion

#### 3.1. Controlled generation of individual dislocation configurations

Figures 1 and 2 are two examples of STM images in Au(001) where nanoindentations of different sizes can be seen. In addition, the two kind of defects observed ~~in Au(001)~~ are shown: ‘mesas’ in Figure 1 and ‘screw-loops’ in Figure 2. ~~Here, we report that these defects can be generated one by one. ‘Mesas’ are rectangular and shallow (0.06 nm high) dislocation configurations whose dislocation structure is also shown. They have also been reproduced under the nanoindentation by atomistic simulations [14,17]. The Burgers vector  $\mathbf{b}$  of a ‘mesa’ configuration is parallel to the surface, along a  $\langle 110 \rangle$  direction. As can be appreciated, these defects can be created in a small number, even individually, like the one generated by the stresses introduced by the nanoindentation on the left. This process of individual generation has also been observed for the defect named ‘screw-loop’ [18]. Figure 2 shows four nanoindentations where terraces of atomic step high are generated around nanoindentations. It shows that nanoindentation patterns can be controlled at the nanometer level. Those terraces ~~(usually referred to as pile-up material)~~ are the traces left on the surface by the gliding and cross-slip of the ‘screw-loops’ (half-loops with the two emerging segments in a screw orientation, their vector  $\mathbf{b}$  being along a  $\langle 110 \rangle$  direction inclined to the surface). ~~The proposed mechanism for the rearrangement of material around the nanoindentation This mechanism for the generation of the pile-up material is confirmed by the observation of dislocations pinned in the course of their gliding as shown in the same figure by an arrow which indicates the point of emergence of a dislocation of screw character  $s$ . Whether both kind of defects (‘mesas’ and ‘screw-loops’) are produced by the same nanoindentation or one of them appears preferentially (like in the examples given) depends on a number of different parameters, specifically on the approach and retraction speed. The detailed mechanism has not been elucidated yet. In all cases, in order to observe defects around the nanoindentation print, it is necessary to apply loads higher than a certain threshold, corresponding to a maximum resolved shear stress (between 2.0 and 6.5 GPa), of the order of the theoretical shear strength. The latter has been estimated earlier by using STM experiments in combination with Hertz’s contact theory [18] and by AFM [15].~~~~

#### 3.2. Spatial distribution of ‘mesas’ around a nanoindentation

Although on a Au(001) surface ‘mesas’ are expected to be present along the two equivalent  $[110]$  and  $[1\bar{1}0]$  directions, the first reported observations [13] showed ‘mesas’ only along one of them. The explanation could be based on a slight deviation of the STM tip from the perpendicular to the surface during the nanoindentation

process and the consequent introduction of higher stresses along one of the two equivalent directions. In our present work, as shown in Figure 3A, ‘mesas’ are present in both  $\langle 110 \rangle$  directions simultaneously. We have also recognised that ‘mesas’ can have their abrupt sides perpendicular or parallel to the direction of the surface reconstruction as shown in Figures 3B and 3C, which are detailed STM images of the Figure 3A. This supports the idea that, contrary to the situation in ion irradiated samples [19-21], reconstruction is not involved in the generation of defects around nanoindentations, at least in the case of ‘mesas’.

‘Mesas’ are emitted around nanoindentations according to a well-defined pattern. After the emission of a *first* ‘mesa’, which eventually is ~~locked~~ pinned at a point of the surface<sup>‡</sup>, perhaps at some kind of pre-existing defect, a successively emitted ‘mesa’ (the *second* ‘mesa’) finds an intermediate stable position at a given distance  $d$  with respect to the nanoindentation trace centre, as shown in Figure 3A.

We try now to find the equilibrium position of the *second* ‘mesa’ by using standard theory of dislocations in a continuum. This position results from a balance between two opposite forces: on the one side, the glide force  $F_{\text{nan}}$  due to the nanoindentation, which tends to force the *second* ‘mesa’ away ~~from it~~ along its glide direction, and, on the other side, a repulsive force  $F_{\text{mesa}}$  between both ‘mesas’ which tries to move back the *second* ‘mesa’ towards the nanoindentation ~~point~~. Although in a previous calculation about the stability of ‘mesas’, the role of the surface was taken into account through the incorporation of image forces [22], the latter have been ignored in the present work on the grounds that the forces arising from them do not have a significant component along the gliding direction of ‘mesas’ (parallel to the surface).

Both forces are computed by using the Peach and Koehler expression for the force per unit length on a dislocation segment of Burgers vector  $\mathbf{b}$ , elementary length  $dl$  lying along the unitary direction  $\xi$ :

$$dF = (\boldsymbol{\sigma} \cdot \mathbf{b} \times \xi) dl \quad (1)$$

where  $\boldsymbol{\sigma}$  is the tensor of the stresses acting on the dislocation segment.

The stress  $\boldsymbol{\sigma}_{\text{nan}}$  due to the nanoindentation is related to the deformation produced by the applied ~~force~~ load,  $P$ , during the nanoindentation process. ~~Taking into account our previously described SEM characterisation of STM tips,~~ We assume that the external force gives rise to an external stress distribution over the contact surface following a Hertz distribution [21],

$$p = p_0 \left[ 1 - \left( \frac{r}{a} \right)^2 \right]^{1/2} \quad (2)$$

where  $p_0 = 3P/2\pi a^2$ ,  ~~$a$  the radius of a circular area of contact,~~ is the maximum external stress and  $r$  the distance from the origin of coordinates to any point  $(x_n, y_n)$  of the nanoindentation trace ( $r^2 = x_n^2 + y_n^2$ ) ~~and  $P$  the applied load.~~ The value of  $a$ , ~~the radius of a circular area of contact,~~ can be written ~~is selected in such a way that the circular area is equal to the area of the nanoindentation trace.~~

$$a = \left( \frac{3PR}{4E^*} \right)^{1/3} \quad (3)$$

<sup>‡</sup> Atomistic simulations [13,17] predict a great mobility of these defects.

where  $R$  the tip radius measured by SEM as described above. Here,  $E^*$  is the effective Young modulus [23], which for a Au(001) sample and a W tip is taken as  $E^* = 78$  GPa. Therefore,

$$p_0 = \left( \frac{6PE^{*2}}{\pi^3 R^2} \right)^{1/3} \quad (4)$$

and it is clear that both  $p_0$  and  $p(r)$  are function of the external load  $P$  only.

The displacement vector  $\mathbf{u}$  produced by the ~~this~~ distributed external force  $p(r)$  can be obtained from the equations from the Green tensor corresponding to a concentrated force in terms of isotropic linear elasticity [24]. The mathematical expressions are:

$$\begin{aligned} u_x &= \Gamma \left( \iint \frac{p(x_n, y_n) \cdot (x_n, y_n) z}{\rho^3} dx_n dy_n - \frac{\mu}{\mu + \lambda} \iint \frac{p(x_n, y_n) \cdot (x - x_n)}{(z + \rho)\rho} dx_n dy_n \right) \\ u_y &= \Gamma \left( \iint \frac{p(x_n, y_n) \cdot (y - y_n) z}{\rho^3} dx_n dy_n - \frac{\mu}{\mu + \lambda} \iint \frac{p(x_n, y_n) \cdot (y - y_n)}{(z + \rho)\rho} dx_n dy_n \right) \quad (5) \\ u_z &= \Gamma \left( \iint \frac{p(x_n, y_n) \cdot z^2}{\rho^3} dx_n dy_n - \frac{2\mu + \lambda}{\mu + \lambda} \iint \frac{p(x_n, y_n)}{\rho} dx_n dy_n \right) \end{aligned}$$

with  $\rho = ((x - x_n)^2 + (y - y_n)^2 + z^2)^{1/2}$ ,  $\Gamma = 1/4\pi\mu$  and  $\mu$  and  $\lambda$  the Lamé coefficients.

By deriving with respect to the  $x, y, z$  coordinates the displacement components (5), one gets the strain tensor,

$$e_{ij} = \frac{1}{2} \left( \frac{\partial u_i}{\partial u_j} + \frac{\partial u_j}{\partial u_i} \right) \text{ and by using Hooke's linear approximation, the stress components } \sigma_{ij} = \lambda e_{mm} \delta_{ij} + 2\mu e_{ij}$$

where  $e_{mm}$  is the trace of the strain tensor.

We can, then, introduce the expression for  $\sigma_{nan}$  into equation (1) and obtain the force on each segment of the *second* 'mesa' for a given distance  $d$  between the nanoindentation and the 'mesa' centre. The total glide force  $F_{nan}(d)$  on ~~the that second~~ 'mesa' due to the nanoindentation stresses (as a function of its distance to the nanoindentation centre) is the sum of the partial forces acting on the five dislocation segments that make up the defect projected along the direction of glide.

In order to estimate the repulsive force  $F_{mesa}(d)$  between both 'mesas', we also use equation (1) while now the stress is  $\sigma_{disl}$ , the ~~one stress~~ created by the dislocation segments of the *first pinned* 'mesa'. Note that calculations are made for a constant separation between the first 'mesa' (the fixed one) and the nanoindentation (the axes origin), the variable being the location of the *second mesa*. The stress tensor associated to a straight finite segment dislocation along the  $Z$  axis (parallel to [001] direction)  $\sigma'$  can be written explicitly [25]. For example, for  $\sigma'_{xx}$ , one has

$$\frac{\sigma'_{xx}}{\sigma_0} = b_x \frac{y}{R(R+\alpha)} \left( 1 + \frac{x^2}{R^2} + \frac{x^2}{R(R+\alpha)} \right) + b_y \frac{x}{R(R+\alpha)} \left( 1 - \frac{x^2}{R^2} - \frac{x^2}{R(R+\alpha)} \right) \quad (6)$$

where  $\alpha = z' - z$  and  $\mathbf{R}$  is a vector linking a dislocation point  $(0, 0, z')$  with a generic point in the solid,  $R^2 = x^2 + y^2 + (z - z')^2$ ,  $b_x$ ,  $b_y$  and  $b_z$  are the three components of the Burgers vector of the segment and  $\sigma_0 = \mu / 4\pi (1 - \nu)$  with  $\mu$  is the shear modulus and  $\nu$  the Poisson ratio. Equations (6) for the stress tensor  $\sigma'$  are correct for segments oriented along the  $Z$  axes. As, in our case, the dislocations segments which make up the 'mesa', are not parallel to this direction, the axis must be rotated and the stress components transformed in the usual way [25]. Finally, equation (1) must be summed over the four segments of the second 'mesa' (we neglect the stair-rod segments because of their short Burgers vector), each term of this sum including a second sum over the stresses created by the four segments of the first 'mesa'. In principle, we should determine 16 components but as we consider 'mesas' of equal size (experimentally these are the usual observed configurations), symmetry considerations reduce the estimate to only 6. The total repulsion force,  $F_{\text{mesa}}(d)$ , is the sum of all the partial forces among the dislocation segments of both 'mesas', projected again along the glide direction. Plotting  $F_{\text{nan}}$  for a given load and  $F_{\text{mesa}}$  as a function of  $d$ , we obtain the intersection of both curves, which defines the equilibrium distance of the second 'mesa' with respect to the centre of the nanoindentation trace (axes origin).

We cannot directly measure  $P$  in our STM experimental set-up but we can estimate it as follows. We plot  $F_{\text{nan}}$  (for a given load  $P$ ) and  $F_{\text{mesa}}$  as a function of  $d$  and we obtain the intersection of both curves. This ~~which~~ defines the equilibrium distance of the second 'mesa' with respect to the centre of the nanoindentation trace (axes origin). Conversely, from the experimentally determined value of the equilibrium distance  $d$ , the value of  $P$  can be estimated. ~~We can now compare the results of the calculation with the experimental findings (Figure 3A).~~ As an example, we take the measured experimental equilibrium distance of the second 'mesa', equal to  $d = 27$  nm in Figure 3A. ~~We have taken~~ From the images of Figure 3A we take the size of the 'mesa'  $7.0 \times 9.0$  nm<sup>2</sup> (MP×PQ in Figure 1). ~~corresponding to the experimental.~~ Plotting  $F_{\text{nan}}$  and  $F_{\text{mesa}}$  for different loads we find that, as shown in Figure 3D, we obtain, then, a load of  $P = 0.8$   $\mu$ N results in such an equilibrium distance. In terms of the Hertz model, the maximum resolved shear stress (in a continuum) corresponding to this load is [26]  $\tau_{\text{max}} = 0.31 p_0$ . Substituting the value of  $p_0$  given by Eq.(3), we obtain  $\tau_{\text{max}} = 1.7$  GPa. ~~It is worth remarking that the above values of  $P_{\text{thres}}$  compare also very well with those obtained by atomistic simulation [11] This is consistent with the values obtained by AFM on comparable samples [15] and values of  $\tau_{\text{max}}$  and that loads of the same order of magnitude have been measured in other nanoindentation experiments [2].~~

Another meaningful comparison can be made in terms of the permanent trace left behind the retracted tip. For the indicated load, Eq.(3) gives the value of  $a = 9.0$  nm, equivalent to Hertz contact area of  $A = 254$  nm<sup>2</sup>. This is in good agreement with the area of the nanoindentation trace left behind by the retracting tip is  $\approx 200$  nm<sup>2</sup>.

~~Although we cannot compare this value directly with the experiment, because we cannot directly measure  $P$  in our STM experimental set-up, we can compare  $P$  with the threshold applied load required to observe plastic deformation at a Au surface [15],  $P_{\text{thres}} \approx 0.5$   $\mu$ N. Nanoindentations, as the one shown in Figure 3A, correspond to loads slightly above the plastic threshold and, therefore, we conclude that our value of  $P \approx 1.6 \times P_{\text{thres}}$  is quite satisfactory.~~

~~It is worth remarking that the above values of  $P_{\text{thres}}$  compare also very well with those obtained by atomistic simulation [11] and that loads of the same order of magnitude have been measured in other nanoindentation experiments [2]. We conclude that our simple model is consistent with the observed spatial~~

~~distribution of ‘mesas’ within a factor of two, which is satisfactory in view of the uncertainties inherent to the process.~~

The above calculation about spatial distribution can be also analysed in conjunction with an earlier one, on whose basis we explained the experimental observation of nucleation of ‘mesas’ along the border of the nanoindentation trace [18], where both a single ‘mesa’ and pairs of ‘mesas’ were nucleated. Both calculations confirm the validity of the dislocation theory for explaining the distribution of defects of dislocation character on the surface of solids. **We conclude that our simple model is consistent with the observed spatial distribution of ‘mesas’ within a factor of two, which is satisfactory in view of the uncertainties inherent to the process.**

### 3.3. ‘Mesas’ motion by nanoindentation

We explore now the characteristics of the dislocation configurations introduced by nanoindentation by investigating their motions under the stresses created by successive indentations. One example of a displacement of ‘mesas’ is shown in Figure 4, where successive nanoindentations have been made on approximately the same point of the surface. The first nanoindentation (A) creates three ‘mesas’ (indicated by the three arrows). After performing a second nanoindentation on top of the first one (B), a ‘mesa’ disappears (presumably, glided out of view) while the rest stay in the same position. A third nanoindentation (C) results in the displacement of the largest ‘mesa’ while the other one remains in its original position. We remark that the motion of the ‘mesa’, *as a whole object*, takes place along the direction of its Burgers vector and confirms the dislocation characteristics of the defect. The amplified images (4D, 4E and 4F) of Figures 4A, 4B and 4C, and their associated depth profiles, show in more detail the structure of these defects. By comparing D and E we can confirm that initially we had two ‘mesas’ locked in the same position of the surface (height of the central area of these defects, 0.12 nm, twice the height of a single ‘mesa’) and that after another nanoindentation, F, the outer ‘mesa’ has moved away (0.06 nm height across the latter). It is worth remarking that ‘mesas’ located in similar “double” positions have also been reproduced by atomistic simulations [27].

Instead of superimposing indentations, pre-introduced ‘mesas’ can be set in motion by performing nanoindentations close to them. For example, after creating a number of ‘mesas’ by a first nanoindentation (Figure 5a), a second nanoindentation, whose trace can be seen at Figure 5b, results in the displacement of ‘mesas’ named with letters A and B along the direction parallel to their abrupt sides. An additional nanoindentation on top of the previous one (Figure 5c) produces a further forward glide of ‘mesa’ A along its Burgers vector’s direction. However, a nanoindentation close to ‘mesas’ C, D and E does not result in any change in their location (Figure 5d).

From the STM images of Figures 4 and 5, we can obtain some interesting conclusions. To move ‘mesas’ (see figures 4B and 4C) the stresses resulting from the nanoindentation have to exceed a certain threshold. Besides, these stresses must result in a significant force along the glide direction of the ‘mesa’. Note, for example, that ‘mesas’ glide in Figure 5B but not in Figure 5D. In the first case, there is a significant component of force (or shear stress) along the glide direction of the defect whereas in the second one, the force resulting from the nanoindentation stresses is acting mainly perpendicular to that glide direction.

It is worth remarking that atomistic simulations [27] show that ‘mesas’ are generated at a certain stress threshold during a stepwise penetration of a spherical repulsive tip. ‘Mesas’, once generated, slip only along the common  $\langle 110 \rangle$  direction contained in the two stacking fault planes (see scheme of Figure 1). They never slip in any other directions, a not unexpected behaviour since extended dislocations can only slip in the plane of the stacking fault.

In summary, ‘mesas’, presumably ~~pinned anchored~~ by some pre-existing surface defect, can be unlocked and set in motion by the operation of external stresses introduced, for example, by subsequent nanoindentations. There must be a significant shear stress along the glide direction of the ‘mesa’ to produce its motion. This first experimental evidence of the motion of ‘mesas’ under stress agrees with atomistic calculations and complements the individual motion of ‘screw-loops’ already shown in previous publications.

### 3.4. Nucleation of terraces associated to ‘screw-loops’

In earlier work we had identified terraces with straight borders parallel to the surface compact directions as associated to the cross-slip of the so-named ‘screw-loops’, the latter introduced by nanoindentation [14]. Atomistic simulations support also the mechanisms involving the generation of this kind of loop [28]. Surprisingly, one often observes terraces of different sign (convex vs concave) around the same nanoindentation as shown in Figure 6A. This figure shows terraces of straight borders along  $\langle 110 \rangle$  directions and 2 nm high but of different sign, i.e. one atomic step high over the surface level (the one at the south-west of the nanoindentation trace) or under it (the one at the south-east). We discuss now how our model based in the theory of dislocations for continuum media can also account for the sign of the terraces.

Figure 7a shows the scheme that we use to study the processes related to terraces formation. We consider the usual  $\{111\}/\langle 110 \rangle$  slip system and a ‘screw-loop’ (drawn for the sake of simplicity like two pure screw segments linked by a mixed one) of Burgers vector  $\mathbf{b} = a \left[ -\frac{1}{2}, 0, \frac{1}{2} \right]$ ,  $a$  being the lattice parameter. A nanoindentation ~~can introduces~~ stresses large enough to ~~produce the generation of these~~ nucleate half-loops and ~~make them glide resulting in originate~~ step terraces like the one shown in the figure. In agreement with the slip system of our crystal and the dislocation configuration geometry we have a step along a  $\langle 110 \rangle$  direction, with a height of  $h = 0.2$  nm. Note that the observed value of  $h$  is equal to the product  $\mathbf{b} \cdot \mathbf{n}$  ( $\mathbf{n}$  being the normal to the surface, along the  $[00\bar{1}]$  direction), which is a further confirmation of the value of  $\mathbf{b}$  for the ‘screw-loop’. Depending on the sign of the Burgers vector, terraces over or under the surface level can obviously be obtained. We argue now that loops with opposite values of  $\mathbf{b}$  can be originated depending on their position with respect to the nanoindentation centre. We calculate the ~~resolved~~ shear stresses,  $\sigma_{\text{res}}$ , acting on the elementary section of a slip plane along the glide direction as a consequence of a nanoindentation. The mathematical expression of  $\sigma_{\text{res}}$  for a point  $(x,y,z)$  inside the crystal is, with  $\underline{\mathbf{b}} = \mathbf{b} / b$ :

$$\sigma_{\text{res}} = (\boldsymbol{\sigma} \cdot \mathbf{n}') \cdot \underline{\mathbf{b}} \quad (7)$$

where  $\mathbf{n}'$  is the slip plane normal. ~~We calculate the averaged resolved shear stress,  $\sigma_{\text{res,av}}$ , by integration of  $\sigma_{\text{res}}$  over the slipped plane and normalising to the unit area.~~ Slip takes place on ~~of~~ an elementary section of the  $\{111\}$  plane, and an elementary loop is nucleated, when the value of  $\sigma_{\text{res}}$  ~~that average value~~ exceeds the critical shear stress necessary to produce the slip along the gliding direction  $\hat{b} = 1/\sqrt{2}[101]$ . After nucleation, ~~the elementary loop can expand by gliding.~~ The sign of  $\sigma_{\text{res}}$   ~~$\sigma_{\text{res,av}}$~~  is an indication of the direction along which the plane slips. If we determine  $\sigma_{\text{res}}$   ~~$\sigma_{\text{res,av}}$~~  at different distances of the origin of the system coordinates (where the nanoindentation is made) and depths, we know its spatial dependence and whether it can change sign for different positions, resulting in the generation of terraces one atomic step over or below the surface. ~~Figures 7b, 7c and 7d~~ shows results of the calculation where the (111) plane has been selected as slip plane

1  
2  
3  
4 ~~and a step of 10 nm long taken along the  $[\bar{1}10]$  direction.~~ The variation of the resolved shear stress  $\sigma_{res}$   ~~$\sigma_{res,av}$~~   
5 with distance is studied along the  $[110]$  direction and different depths. It can be checked that  $\sigma_{res}$   ~~$\sigma_{res,av}$~~   
6 changes ~~of~~ sign both with distance and with depth for all the cases; this demonstrates the possibility of  
7 generation of terraces of different signs. This calculation has been done for a nanoindentation force of  $F = 10$   
8  $\mu\text{N}$  well beyond the threshold to initiate plasticity and to generate stable defects on the surface.  
9

10  
11 We discuss now the shape of the permanent concave traces around the nanoindentation centre. In some  
12 cases, also protruding mounds appear (as in Figure 6A). A number of processes take place in the  
13 nanoindentation: we have verified the formation of a neck of gold during the contact of the tungsten tip and  
14 the surface sample in agreement with other experiments and simulations [7], [29-34]. The rupture of the neck,  
15 when both solids are separated after the nanoindentation is made, could indeed produce the previously  
16 referred mounds. Furthermore, protrusions on the surface when metallic tips touch the surface of metals have  
17 been previously observed [28-31], although no additional defects on the surface have been reported. Apart  
18 from these well-characterised processes, we have also observed that, as the size of the nanoindentation traces  
19 increase, these traces tend to show straight borders (with side parallel to  $\langle 110 \rangle$  surface directions), similar to  
20 the terraces generated by 'screw-loops'. We argue that our model involving dislocation nucleation and further  
21 cross-slip is also valid for explaining the shape of the rectangular nanoindentation traces of the Figure 6B and  
22 the several straight-sided terraces shaping the inside of the trace. Indeed, the straight side traces originated  
23 from nanoindentations with an STM tip are also observed along the crystallographic compact directions in our  
24 AFM experiments [15] with a pyramidal tip. This seems evidence that permanent traces (and the  
25 corresponding dislodging and transport of matter) at the nanoindentation contact, rather than from purely  
26 diffusive processes, arise from a dislocation mechanism implying cross-slip of dislocation loops with a screw-  
27 component.  
28  
29  
30  
31

## 32 Conclusions

33  
34 We have shown that **incipient plastic** involving glide, and often cross-slip, of special dislocation  
35 configurations called 'mesas' and 'screw-loops' are in operation around nanoindentations in Au. **The former**  
36 **are related to mass transport along the surface away from the nanoindentation point, while the latter account**  
37 **for the pileup material.** These dislocation mechanisms seem more efficient than surface diffusion for mass  
38 transport around nanoindentations. They also account for the shape of permanent traces of dislodged material  
39 showing rectangular shapes along the compact directions of the surface, independently of the tip shape. We  
40 have recognised the emission of 'mesas' as individual processes taking place at the initial stages of plastic  
41 deformation near the surface. It has been experimentally shown that both 'mesas' and 'screw-loops' can be  
42 unlocked from their positions and set into glide motion by external stresses conveyed by subsequent  
43 nanoindentations performed in their neighbourhood. We have demonstrated that the theory of elasticity in an  
44 isotropic continuum can be used to explain not only the dislocation parameters of 'mesas' and 'screw-loops'  
45 but also the interactions between these defects along with other observations, for example, the spatial  
46 distribution of 'mesas' resulting from the equilibrium between the stresses originated from the  
47 nanoindentation itself and those arising from the interaction with other defects.  
48  
49  
50  
51

## 52 Acknowledgments

53  
54 The grant n° MAT2003-08627-C02-01 from the Spanish Ministry of Science and Technology (MCYT) is  
55 gratefully acknowledged. E.C. thanks the same Ministry for a graduate scholarship.  
56  
57  
58  
59  
60

## References

- [1] S.G. Corcoran, R.J. Colton, E.T. Lilleoden, *et al.*, Phys. Rev. B **55** R16057 (1997).
- [2] J.D. Kiely, and J.E. Houston, Phys. Rev. B **57** 12588 (1998).
- [3] J. Li, K.J. Van Vliet, T. Zhu, *et al.*, Nature **418** 307 (2002).
- [4] K.J. Van Vliet, J. Li, T. Zhu, *et al.*, Phys. Rev. B **67** 104105-1 (2003).
- [5] R. Smith, D. Christopher, S.D. Kenny, *et al.*, Phys. Rev. B **67** 245405-1 (2003).
- [6] T. Filleter, S. Maier and R. Bennewitz, Phys. Rev. B **73** 155433-1 (2006).
- [7] U. Landman, W.D. Luedtke, N.A. Burnham, *et al.*, Science **248** 454 (1990).
- [8] J.A. Zimmerman, C.L. Kelchner, P.A. Klein, *et al.*, Phys. Rev. Lett. **87** 165507-1 (2001).
- [9] E.T. Lilleodden, J.A. Zimmerman, S.M. Foiles *et al.*, J. Mech. Phys. Solids **51** 901 (2003).
- [10] D. Feichtinger, P.M. Derlet and H. Van Swygenhoven, Phys. Rev. B **67** 024113-1 (2003).
- [11] J. Knap and M. Ortiz, Phys. Rev. Lett. **90** 226102-1 (2003).
- [12] J. de la Figuera, M.A. González, R. García-Martínez, *et al.*, Phys. Rev. B **58** 1169 (1998).
- [13] O. Rodríguez de la Fuente, J.A. Zimmerman, M.A. González, *et al.*, Phys. Rev. Lett. **88** 036101-1 (2002).
- [14] E. Carrasco, O. Rodríguez de la Fuente, M.A. González, *et al.*, Phys. Rev. B (Rapid Commun.) **68** 180102-1(R) (2003).
- [15] A. Asenjo, M. Jafaar, E. Carrasco, *et al.*, Phys. Rev. B **73** 075431-1 (2006).
- [16] E. Carrasco, O. Rodríguez de la Fuente, M.A. González, *et al.*, Eur. Phys. J. B **40** 421 (2004).
- [17] F. El Gabaly, R. Miranda and J. de la Figuera, Phys. Rev. B **70** 012102-1 (2004).
- [18] E. Carrasco, O. Rodríguez de la Fuente, M.A. González, *et al.*, Surf. Sci. **572** 467 (2004).
- [19] M. A. González, J. de la Figuera, O. Rodríguez de la Fuente, *et al.*, Surf. Sci. Lett. **429** L486 (1999).
- [20] O. Rodríguez de la Fuente, M.A. González, J.M. Rojo, Surf. Sci., **454-456** 16 (2000).
- [21] O. Rodríguez de la Fuente, M.A. González, J.M. Rojo, Phys. Rev. B **63** 085420 (2001).
- [22] O. Rodríguez de la Fuente, M.A. González, J.M. Rojo, Phil. Mag. **83** 485 (2003).
- [23] K.L. Johnson, *Contact Mechanics*, (Cambridge University Press, Cambridge 1985), pp. 92.
- [24] L. D. Landau and E. M Lifshitz, *Theory of Elasticity*, (Pergamon, New York 1959) pp. 29.
- [25] J.P. Hirth and J. Lothe, *Theory of Dislocations*, (2<sup>nd</sup> ed., John Wiley & Sons, New York 1982), pp. 134.
- [26] K.L. Johnson, *ibid*, pp. 155.
- [27] O. Rodríguez de la Fuente, *Progress in Industrial Mathematics at ECMI 2006*, L.L. Bonilla *et al.* (eds.), Springer, 2007.
- [28] C.L. Kelchner, S.J. Plimpton and J.C. Hamilton, Phys. Rev. B **58** 11085 (1998).
- [29] J.K. Gimzewski and R. Möller, Phys. Rev. B (Rapid Commun.) **36** 1284 (1987).
- [30] L. Olesen, E. Lægsgaard, I. Stensgaard, *et al.*, Phys. Rev. Lett. **72** 2251 (1994).
- [31] J.I. Pascual, J. Méndez, J. Gómez-Herrero, *et al.*, Phys. Rev. Lett. **71** 1852 (1993).
- [32] C. Untiedt, G. Rubio, S. Vieira, *et al.*, Phys. Rev. B **56** 2154 (1997).
- [33] P. Jelínek, R. Pérez, J. Ortega, *et al.*, Phys. Rev. B **68** 085403-1 (2003).
- [34] Y. Sun, H. Mortensen, S. Schär, *et al.*, Phys. Rev. B **71** 193407-1 (2005).

## Figure captions

Figure 1. STM image (150x150 nm<sup>2</sup>) of the Au(001) surface after two nanoindentations made with the STM tungsten tip. The smallest nanoindentation (on the left) has been performed with a bias voltage of -0.40 V and the second nanoindentation with a bias voltage of -0.35 V. This tunnelling parameter allows the regulation of nanoindentation sizes. Both nanoindentations have created 'mesas'. The glide direction of these dislocation configurations is indicated by a white arrow. Below: dislocation model proposed for a 'mesa', with emerging points M, N, M' and N'. The subsurface structure consists of two stacking faults (dark grey) on

intersecting  $\{111\}$  planes each bounded by two parallel Shockley partial dislocations (with Burgers vectors  $\beta D$ ,  $C\beta$ ,  $\alpha D$  and  $C\alpha$ , in the Thompson notation). The whole configuration is held up by a stair-rod dislocation parallel to the surface ( $\alpha\beta$ ).

Figure 2. STM Image ( $600 \times 600 \text{ nm}^2$ ) of four successive nanoindentations on Au(001). In all cases, terraces of straight edges in the neighbourhood of the nanoindentations can be observed. Also, a pinned dislocation with a screw component perpendicular to the surface is visible ( $s$  indicates the emergent point of that dislocation). Although most of the terraces follow  $\langle 110 \rangle$  directions, some terraces have borders along the  $\langle 100 \rangle$  direction (indicated by arrows). The height of all the terraces is 0.2 nm; terraces can be either over or under the surface level. **Below: scheme of a model screw-loop, in Thompson notation, after one cross-slip event below a (001) surface. The half loop, with total Burgers vector DA and dissociated into two partial dislocations, initially nucleates in plane (b) and cross-slips to plane (c), dragging a surface step (dashed lines). At the intersection of both planes a stair-rod dislocation ( $\gamma\beta/AD$ ) is formed. The emerging points of the dissociated screw dislocations are signaled with S, as in the STM image. All the Burgers vectors of the four Shockley and the stair-rod partial dislocations are shown. Two additional consecutive cross-slip events in the same winding direction would finally form a surface crystallographic terrace as those shown in the STM image.**

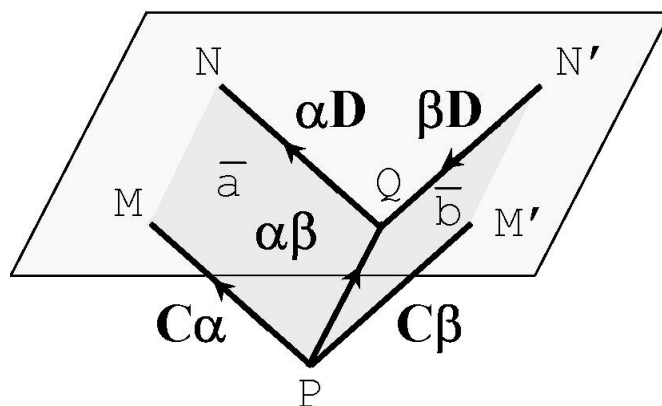
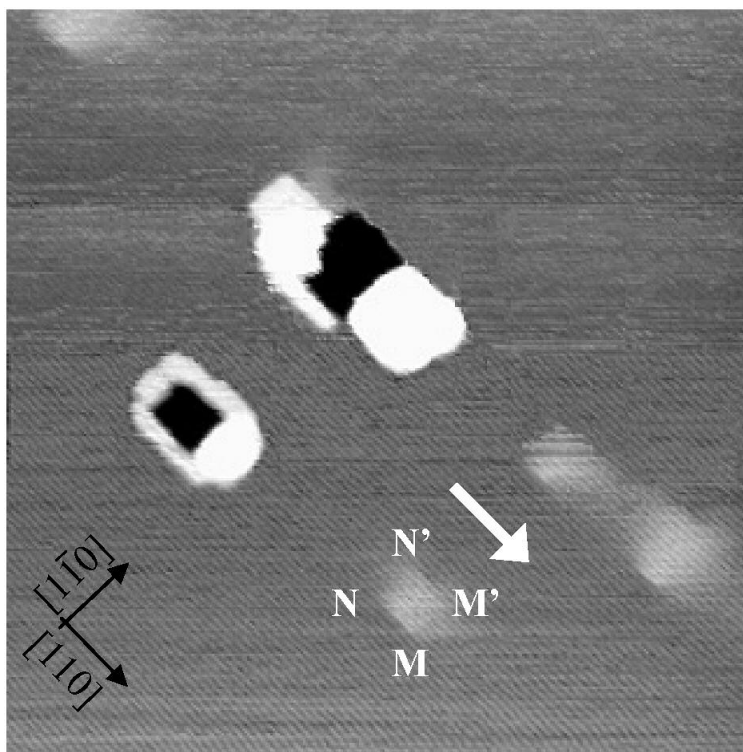
Figure 3. A) STM image ( $130 \times 130 \text{ nm}^2$ ) of the area around a nanoindentation. It gives evidence of simultaneous generation of 'mesas' along both  $\langle 110 \rangle$  surface directions, in agreement with previous atomistic simulations [24]. B) and C) Magnified images of  $27 \times 27 \text{ nm}^2$  and  $40 \times 40 \text{ nm}^2$ , respectively, where the structure of the 'mesas' can be appreciated in more detail. D) Graphic of the computed forces acting along the direction of gliding on the *second* 'mesa' 2. The continuous line represents, for a load of  $P = 0.8 \mu\text{N}$ , the force due arising from nanoindentation stresses,  $F_{nan}$ , and the dotted line the force originated from the repulsion between the two 'mesas',  $F_{mesa}$ . The intersection point of both graphs give us the equilibrium position of the *second* 'mesa' with respect to the centre of the nanoindentation trace:  $d = 27 \text{ nm}$ .

Figure 4. A), B) and C) show successive nanoindentations on the same point of a Au(001) surface ( $200 \times 200 \text{ nm}^2$ ). After this first nanoindentation, three 'mesas' can be observed (signalled with arrows). The second nanoindentation (B) results in the disappearance of one the 'mesas' while the other two keep the same position. After a third nanoindentation, the largest 'mesa' moves as a whole along a  $\langle 110 \rangle$  direction. D), E), and F) show magnified images ( $80 \times 80 \text{ nm}^2$ ) of these 'mesas' (corresponding respectively to the STM images A), B) and C)), together with their height profiles.

Figure 5. Examples of nanoindentations performed on the proximity of 'mesas' generated by previous nanoindentations. (a) 'Mesas' created at different positions and orientations by nanoindentation. (b) Image showing the displacement of 'mesas' A and B (inside a circle to help identification) due to a nanoindentation performed close to them. (c) Another nanoindentation on the same point of the previous nanoindentation produces an additional movement of 'mesa' A. (d) On the contrary, a new nanoindentation (on the left of the image) does not induce any displacement of three 'mesas' situated next to it. Not only the value of the applied forces but also the orientation of the 'mesas' is important to produce the motion of the latter.

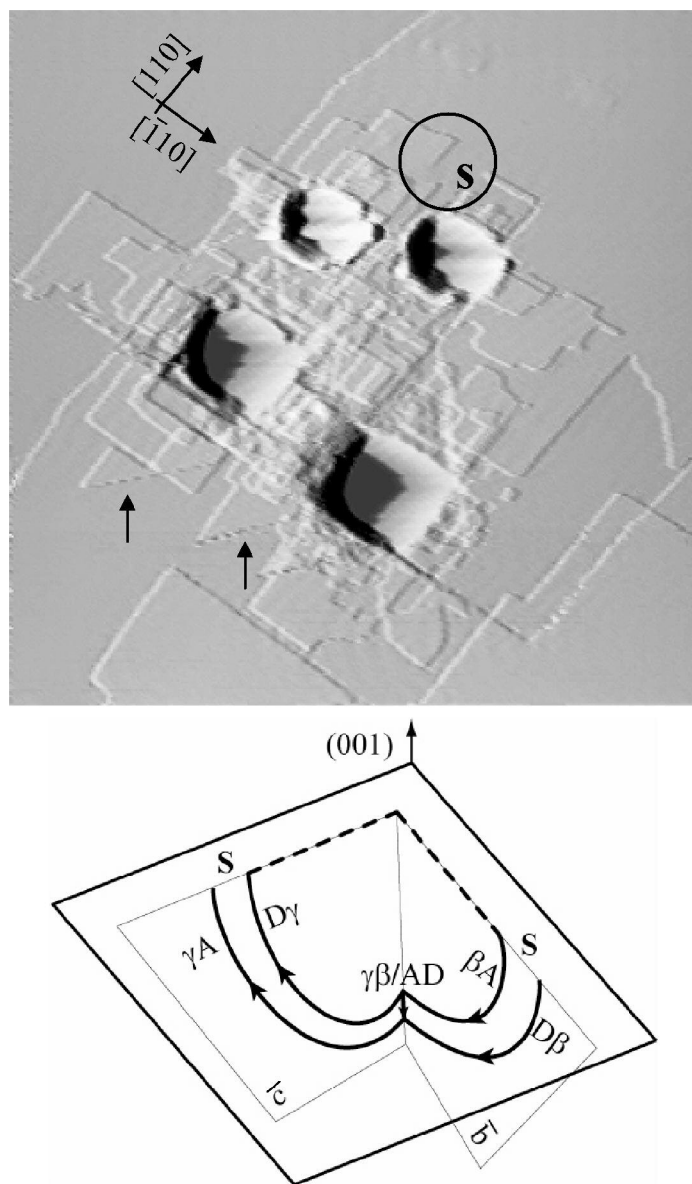
Figure 6. A) Image ( $180 \times 180 \text{ nm}^2$ ) of a nanoindentation on Au(001) where two terraces of an atomic height over and under the surface have been created. One of these terraces, which crosses three surface steps, is 0.2 nm higher than its surroundings whereas the other is 0.2 nm deeper than the surface level. B) Another STM image of a nanoindentation ( $150 \times 150 \text{ nm}^2$ ) where new terraces are created. In this case, it can be clearly seen the rectangular shape of the nanoindentation print and several straight terraces inside the print. It is worth noting that two steps created on the surface prior to the indentation have been modified by the 'screw-loops' originated thereafter (indicated with arrows).

Figure 7. a) Scheme explaining the formation of terrace steps resulting from the 'screw-loop' slip on  $\{111\}$  planes under the shear stresses introduced by a nanoindentation. We calculate the resolved shear  $\sigma_{res}$  acting on the elementary section of a (111) plane (where an elementary loop is nucleated) along the glide direction (for the (111) plane along the  $[\bar{1}01]$  gliding direction) averaged for an elementary section of plane,  $\sigma_{eff}$ . The elementary loop can expand and glide, resulting in a step terrace oriented along the glide direction  $[\bar{1}10]$ . The elementary area of plane corresponds to a step oriented along the direction and 10 nm long. B), C) and D) b) The graph shows the variation of  $\sigma_{res} = \sigma_{eff}$  with distance from the centre of application of a point force  $P$  of 10  $\mu\text{N}$  at three different depths:  $z = 0.5 \text{ nm}$ , 5 nm and 15 nm, respectively. A change of sign of this stress with distance and depth can be observed. This result explains the different sign of the concavity of terraces observed with STM.



**Figure 1.** STM image ( $150 \times 150 \text{ nm}^2$ ) of the Au(001) surface after two nanoindentations made with the STM tungsten tip. The smallest nanoindentation (on the left) has been performed with a bias voltage of  $-0.40 \text{ V}$  and the second nanoindentation with a bias voltage of  $-0.35 \text{ V}$ . This tunnelling parameter allows the regulation of nanoindentation sizes. Both nanoindentations have created 'mesas'. The glide direction of these dislocation configurations is indicated by a white arrow. Below: dislocation model proposed for a 'mesa', with emerging points M, N, M' and N'. The subsurface structure consists of two stacking faults (dark grey) on intersecting  $\{111\}$  planes each bounded by two parallel Shockley partial dislocations (with Burgers vectors  $\beta_D$ ,  $C\beta$ ,  $\alpha_D$  and  $C\alpha$ , in the Thompson notation). The whole configuration is held up by a stair-rod dislocation parallel to the surface ( $\alpha\beta$ ).

79x126mm (300 x 300 DPI)



**Figure 2. STM Image ( $600 \times 600 \text{ nm}^2$ ) of four successive nanoindentations on Au(001). In all cases, terraces of straight edges in the neighbourhood of the nanoindentations can be observed. Also, a pinned dislocation with a screw component perpendicular to the surface is visible (s indicates the emergent point of that dislocation). Although most of the terraces follow directions  $\langle 110 \rangle$ , some terraces have borders along the direction  $\langle 100 \rangle$  (indicated by arrows). The height of all the terraces is 0.2 nm; terraces can be either over or under the surface level. Below: scheme of a model screw-loop, in Thompson notation, after one cross-slip event below a (001) surface. The half loop, with total Burgers vector  $DA$  and dissociated into two partial dislocations, initially nucleates in plane (b) and cross-slips to plane (c), dragging a surface step (dashed lines). At the intersection of both planes a stair-rod dislocation  $(\gamma\beta/AD)$  is formed. The emerging**

1  
2  
3 **points of the dissociated screw dislocations are signalled with S, as in the STM image. All**  
4 **the Burgers vectors of the four Shockley and the stair-rod partial dislocations are shown.**  
5 **Two additional consecutive cross-slip events in the same winding direction would finally**  
6 **form a surface crystallographic terrace as those shown in the STM image.**

7 96x162mm (300 x 300 DPI)  
8  
9  
10  
11  
12  
13  
14  
15  
16  
17  
18  
19  
20  
21  
22  
23  
24  
25  
26  
27  
28  
29  
30  
31  
32  
33  
34  
35  
36  
37  
38  
39  
40  
41  
42  
43  
44  
45  
46  
47  
48  
49  
50  
51  
52  
53  
54  
55  
56  
57  
58  
59  
60

For Peer Review Only

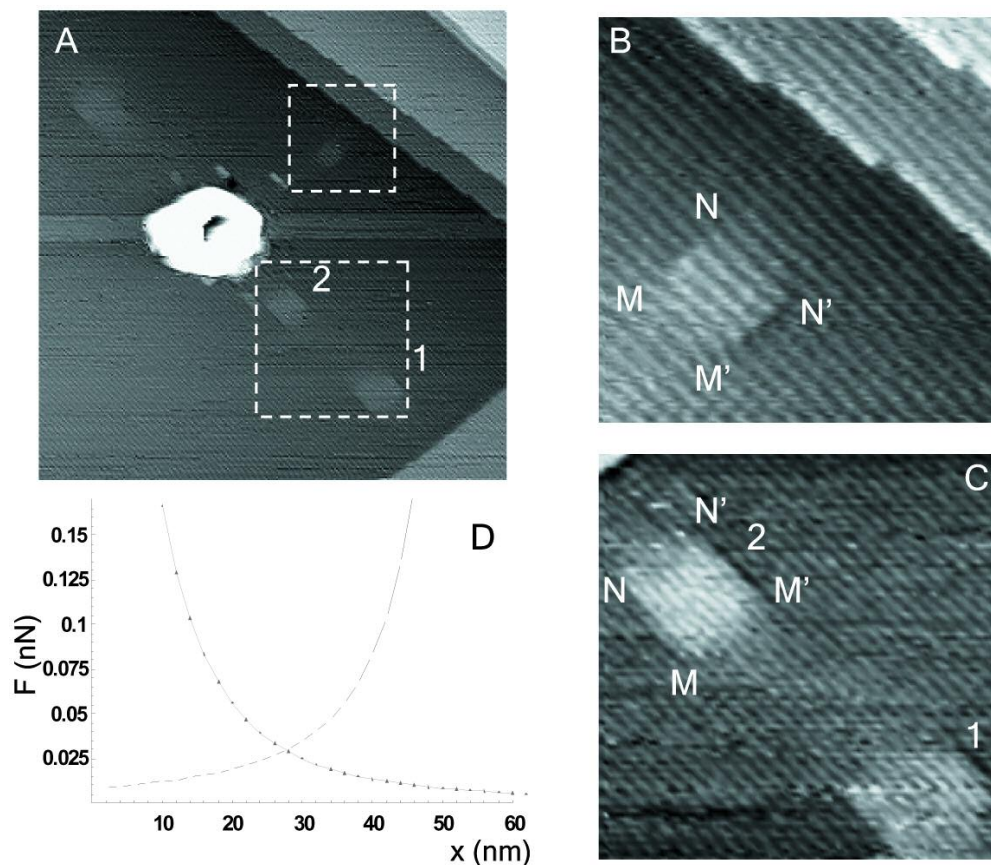


**Figure 3. A) STM image ( $130 \times 130 \text{ nm}^2$ ) of the area around a nanoindentation. It gives evidence of simultaneous generation of 'mesas' along both surface directions, in agreement with previous atomistic simulations [24]. B) and C) Magnified images of  $27 \times 27 \text{ nm}^2$  and  $40 \times 40 \text{ nm}^2$ , respectively, where the structure of the 'mesas' can be appreciated in more detail. D) Graphic of the computed forces acting along the direction of gliding on the second 'mesa' 2. The continuous line represents, for a load of  $P = 0.8 \mu\text{N}$ , the force due arising from nanoindentation stresses,  $F_{\text{nan}}$ , and the dotted line the force originated from the repulsion between the two 'mesas',  $F_{\text{mesa}}$ . The intersection point of both graphs give us the equilibrium position of the second 'mesa' with respect to the centre of the nanoindentation trace:  $d = 27 \text{ nm}$ .**

407x351mm (72 x 72 DPI)

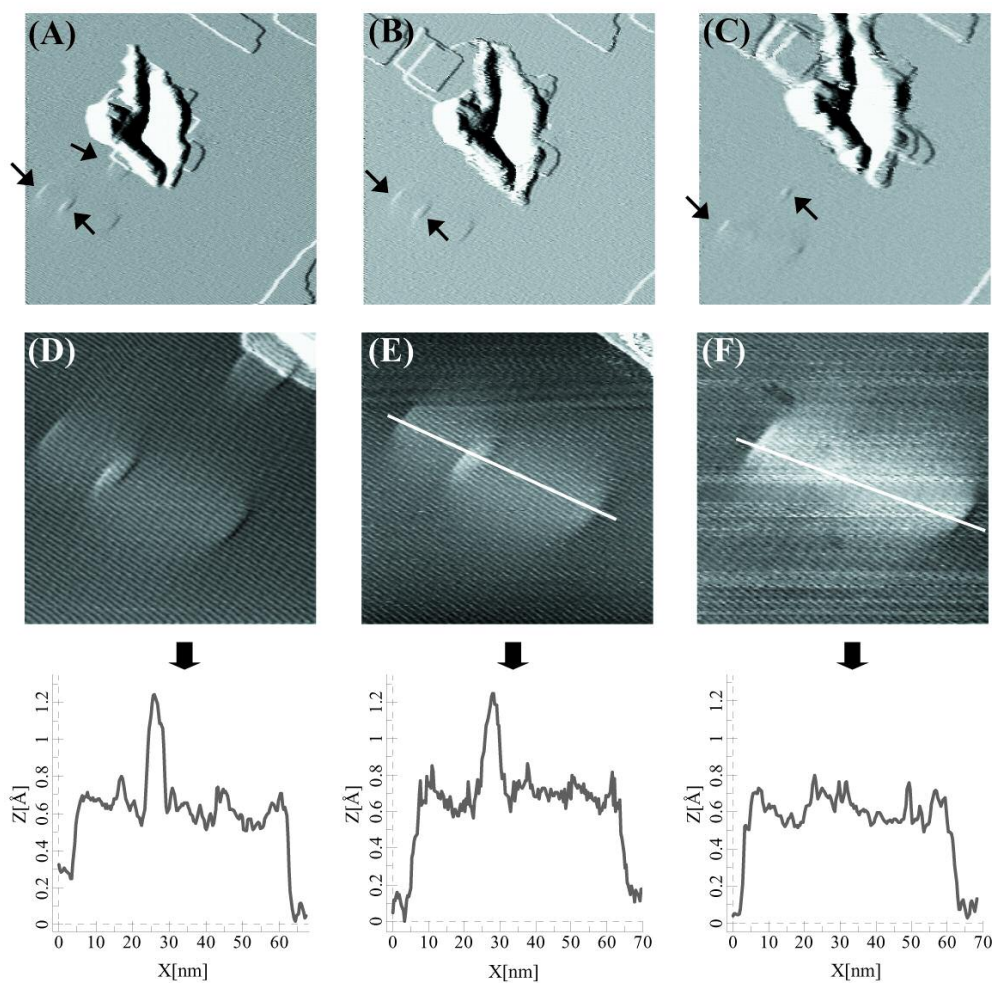


**Figure 4. A), B) and C) show successive nanoindentations on the same point of a Au(001) surface ( $200 \times 200 \text{ nm}^2$ ). After this first nanoindentation, three 'mesas' can be observed (signalled with arrows). The second nanoindentation (B) results in the disappearance of one the 'mesas' while the other two keep the same position. After a third nanoindentation, the largest 'mesa' moves as a whole along a direction  $\langle 110 \rangle$ . D), E), and F) show magnified images ( $80 \times 80 \text{ nm}^2$ ) of these 'mesas' (corresponding respectively to the STM images A), B) and C)), together with their height profiles.**

410x402mm (72 x 72 DPI)

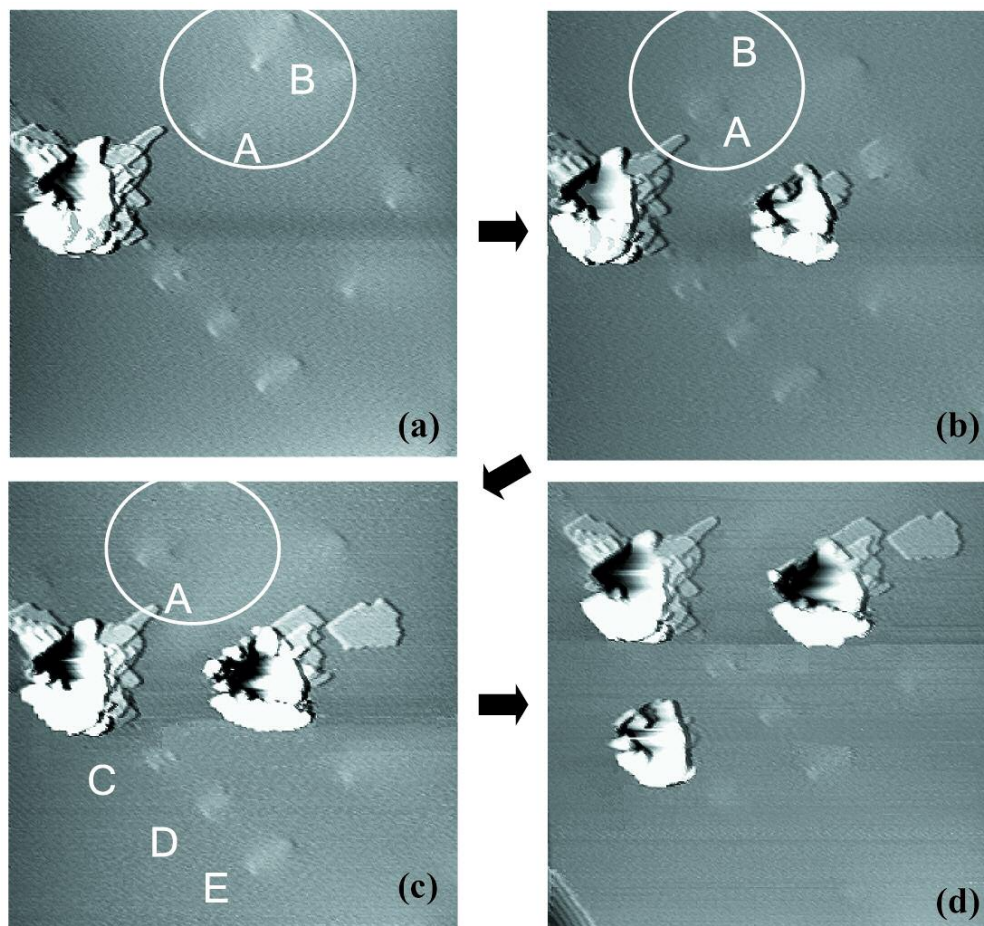


**Figure 5. Examples of nanoindentations performed on the proximity of 'mesas' generated by previous nanoindentations. (a) 'Mesas' created at different positions and orientations by nanoindentation. (b) Image showing the displacement of 'mesas' A and B (inside a circle to help identification) due to a nanoindentation performed close to them. (c) Another nanoindentation on the same point of the previous nanoindentation produces an additional movement of 'mesa' A. (d) On the contrary, a new nanoindentation (on the left of the image) does not induce any displacement of three 'mesas' situated next to it. Not only the value of the applied forces but also the orientation of the 'mesas' is important to produce the motion of the latter.**

390x364mm (72 x 72 DPI)

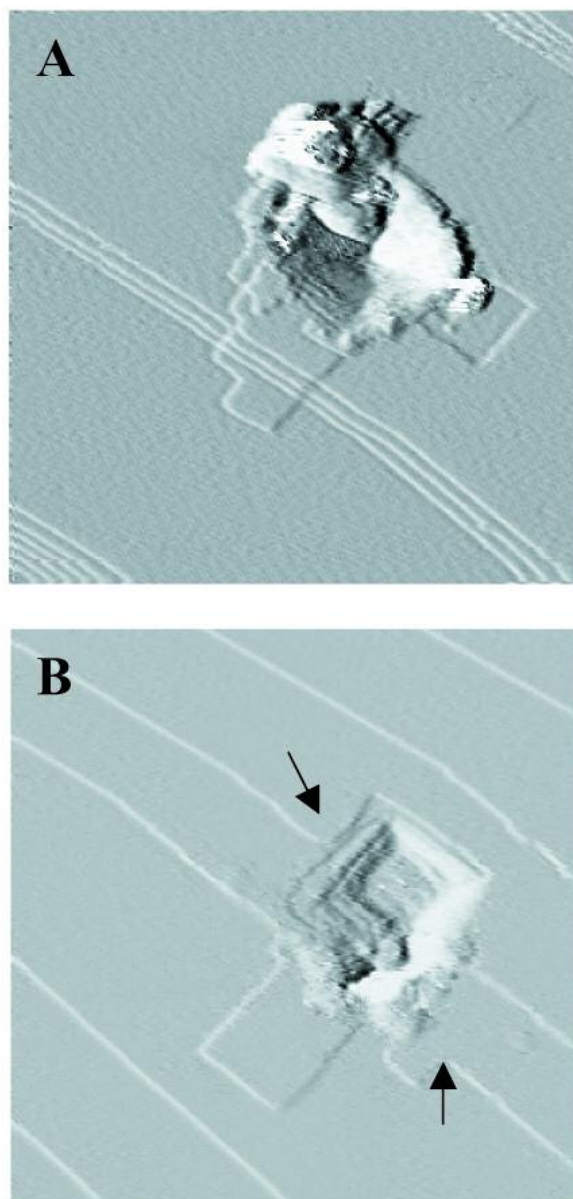


**Figure 6. A) Image ( $180 \times 180 \text{ nm}^2$ ) of a nanoindentation on Au(001) where two terraces of an atomic height over and under the surface have been created. One of these terraces, which crosses three surface steps, is 0.2 nm higher than its surroundings whereas the other is 0.2 nm deeper than the surface level. B) Another STM image of a nanoindentation ( $150 \times 150 \text{ nm}^2$ ) where new terraces are created. In this case, it can be clearly seen the rectangular shape of the nanoindentation print and several straight terraces inside the print. It is worth noting that two steps created on the surface prior to the indentation have been modified by the 'screw-loops' originated thereafter (indicated with arrows).**

153x312mm (72 x 72 DPI)

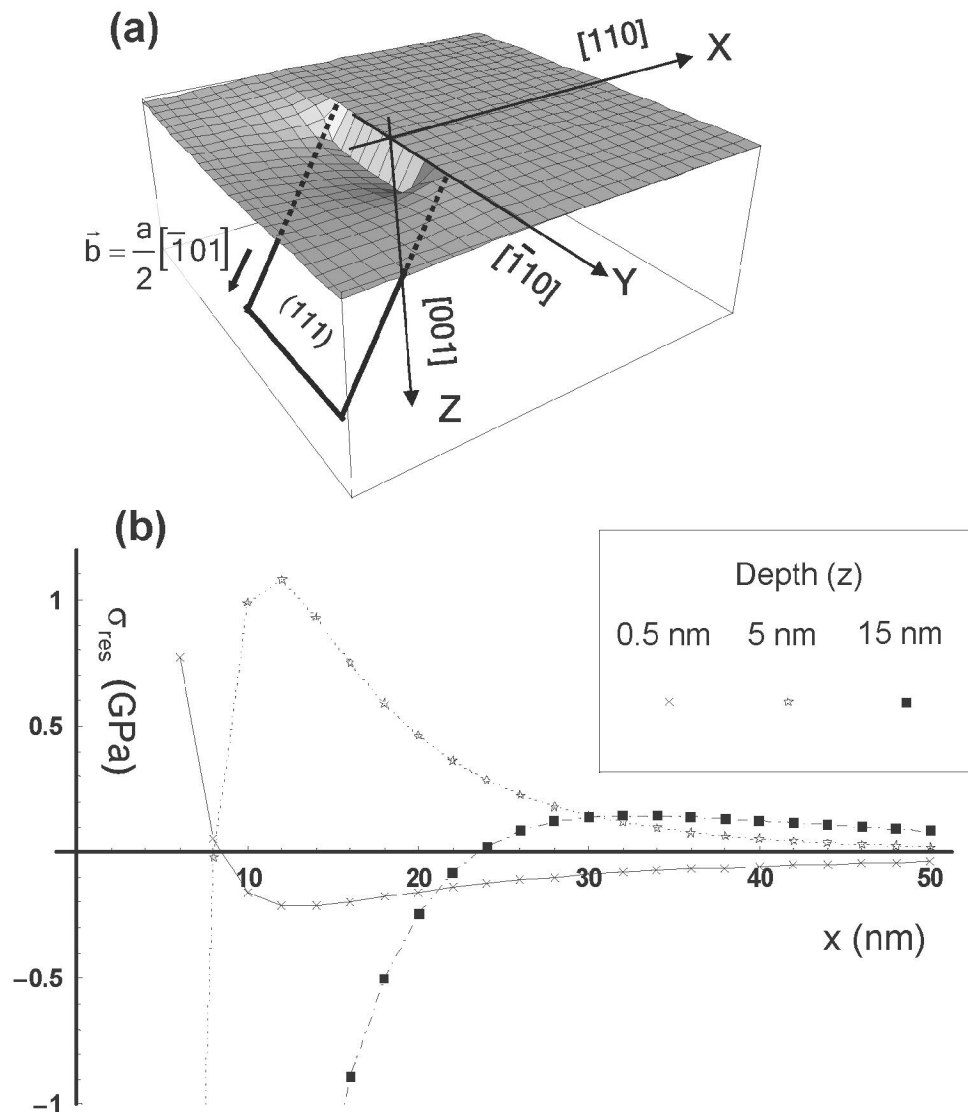


**Figure 7. a) Scheme explaining the formation of terrace steps resulting from the 'screw-loop' slip on  $\{111\}$  planes under the shear stresses introduced by a nanoindentation. We calculate the resolved shear stress  $\sigma_{res}$  acting on the elementary section of a (111) plane (where an elementary loop is nucleated) along the glide direction  $\langle -101 \rangle$ . The elementary loop can expand and glide, resulting in a step terrace oriented along the  $\langle -110 \rangle$  direction. b) The graph shows the variation of  $\sigma_{res}$  with distance from the centre of application of a point force  $P$  of  $10 \mu\text{N}$  at three different depths:  $z = 0.5 \text{ nm}$ ,  $5 \text{ nm}$  and  $15 \text{ nm}$ , respectively. A change of sign of this stress with distance and depth can be observed. This result explains the different sign of the concavity of terraces observed with STM.**

135x159mm (300 x 300 DPI)

1  
2  
3  
4  
5  
6  
7  
8  
9  
10  
11  
12  
13  
14  
15  
16  
17  
18  
19  
20  
21  
22  
23  
24  
25  
26  
27  
28  
29  
30  
31  
32  
33  
34  
35  
36  
37  
38  
39  
40  
41  
42  
43  
44  
45  
46  
47  
48  
49  
50  
51  
52  
53  
54  
55  
56  
57  
58  
59  
60

For Peer Review Only